SURFACE-ENGINEERED METALLIC AND POLYMERIC MATERIALS PROMOTE OSTEOBLAST-LIKE CELL ADHESION, GROWTH AND DIFFERENTIATION FOR ORTHOPEDIC AND SPINE SURGERY APPLICATIONS

Lucie Bačáková[1,2]*, Chadi Ali[1], Marta Vandrovcová[1], Lubica Staňková[1], Ivana Němčáková[1], Ondřej Kylián[3], Zdeněk Čejka[4]

[1]Laboratory of Biomaterials and Tissue Engineering, Institute of Physiology of the Czech Academy of Sciences, Vídeňská 1083, 142 00 Prague 4 - Krč, Czech Republic

[2]Faculty of Materials and Technology, VSB-Technical University of Ostrava, 17. listopadu 2172/15, 708 00 Ostrava, Czech Republic

[3]Department of Macromolecular Physics, Faculty of Mathematics and Physics, Charles University, V Holešovičkách 747/2, 180 00 Prague 8, Czech Republic

[4]Prospon spol. s. r. o., Jiřího Voskovce 3206, 272 01 Kladno, Czech Republic

[$]Present address: Royal National Orthopaedic Hospital (RNOH) NHS Trust, Brockley Hill, Stanmore, Middlesex, HA7 4LP, United Kingdom

Abstract

Materials commonly used in orthopedic, dental and spine surgeries—including Ti-6Al-4V alloy, stainless steel AISI 316 LWM, polyether ether ketone (PEEK) Optima, and ultra-high molecular weight polyethylene (UHMWPE)—were subjected to surface modifications such as sandblasting, polishing, and coating with amorphous hydrogenated carbon (a-C:H), alone or in combination. Surface roughness, assessed by the R_a parameter, was primarily at the submicron scale for unmodified or sandblasted materials and at the nanoscale for polished samples. Wettability and the polar component of surface energy were generally higher on metallic samples and standard polystyrene culture dishes than on polymeric materials, with the exception of polished stainless steel. When seeded with human osteoblast-like MG-63 cells, the highest cell densities were observed on sandblasted Ti-6Al-4V coated with a-C:H (day 1), polished stainless steel (day 3), and polished PEEK (day 8). These cells also displayed elevated levels of adhesion and osteogenic differentiation markers, including β_1-integrins (on sandblasted Ti-6Al-4V with a-C:H), α_v-integrins, vinculin, and osteocalcin (on polished stainless steel), and talin and osteopontin (on polished PEEK). Furthermore, the cells on all tested materials exhibited comparable or lower levels of intercellular adhesion molecule-1 (ICAM-1), an immune activation marker, compared to those grown on standard polystyrene dishes. These findings suggest that sandblasted Ti-6Al-4V coated with a-C:H, polished stainless steel, and polished PEEK are promising materials for bone implant construction and osseointegration.

Keywords: *bone implants, metals, polymers, osteoblasts, adhesion, proliferation, osteogenic differentiation, inflammatory activation*

1. INTRODUCTION

Early osteointegration of materials used for bone implants—such as metals, polymers, and ceramics—depends primarily on the formation of new bone tissue apposing the material surface. Based on their ability to stimulate bone formation, these materials can be broadly classified as bioinert or bioactive.

Bioinert materials are tolerated by surrounding tissues but do not actively promote bone formation. Instead, they may induce fibrous tissue formation, resulting in a weak biomaterial-bone interface without direct bone bonding. Nonetheless, bioinert materials are useful for temporary bone implants, such as external or internal fixators, where ease of removal is critical.

Most metallic and synthetic polymeric materials currently employed for bone implantation are bioinert in their unmodified state. Examples include titanium and its alloys [1–3], stainless steel [4], PEEK [5],

UHMWPE [6, 7], and some ceramics such as alumina and zirconia [8]. In contrast, phosphate-based ceramics [9], bioactive glass [10, 11], and nature-derived polymers—like collagen, chitosan, fibronectin, vitronectin [12], gelatin [13], and hyaluronic acid [14]—exhibit bioactive properties.

The osseointegration of bioinert materials can be enhanced by various surface modifications, which can be subtractive, additive, or a combination of both [2, 12]. Subtractive methods include grinding, polishing, machining, sandblasting, grit blasting, acid or alkaline etching, and shot peening [15–18]. Additive approaches typically involve coating the surface with organic or inorganic bioactive films, such as carbon-based layers (nanocrystalline diamond, graphene), ceramic films containing phosphate-based ceramics, TiO_2 [12, 18], or bioactive glass, sometimes combined with strontium [11]. Materials can also be coated with synthetic or natural polymer films that mediate cell adhesion [12], or functionalized with cell adhesion oligopeptides [19] and bone morphogenetic proteins [20].

Both subtractive and additive modifications primarily enhance surface bioactivity by altering physicochemical properties such as wettability, roughness, topography, electric charge, and conductivity [2, 12, 21]. Surface roughness is a critical factor for implant osseointegration. Macroscopic roughness facilitates mechanical anchoring without impeding bone cell adhesion and growth. However, the influence of microscale roughness on osteoblast adhesion and proliferation is more nuanced; micrometer-scale irregularities can sometimes hinder cell spreading, which is essential for proliferation [12, 21]. Nonetheless, micro-rough surfaces generally promote osteogenic differentiation [16, 22].

Nanoscale surface roughness is especially important as it mimics the irregularities of the natural extracellular matrix (ECM), promoting adsorption of ECM molecules in conformations favorable for recognition by cell adhesion receptors. Additionally, nanoscale roughness enhances surface wettability, further supporting cell adhesion and growth [2, 3, 21, 23]. Both subtractive and additive modifications also improve mechanical and chemical resistance of materials. For instance, polishing carbon fiber-reinforced carbon composites improved osteoblast-like and vascular cell adhesion and growth while reducing particle release [15]. Similar benefits were observed in Ti-6Al-4V alloy treated by chemical milling and shot peening [17]. Coatings of carbon-based or ceramic films also improve mechanical, tribological, and anticorrosion properties, while controlling cell adhesion and growth [1, 12, 18].

In this study, we investigated bioactive surface modifications of metallic and polymeric materials used in bone implants, joint replacements and spine surgery, including Ti-6Al-4V alloy, AISI 316LVM stainless steel, PEEK, and UHMWPE. Metallic materials were modified by sandblasting or polishing, followed by coating with amorphous hydrogenated carbon (a-C:H), a member of the diamond-like carbon (DLC) family [24, 25]. Polymeric materials were either left unmodified or polished. The materials were characterized by their surface roughness, wettability, and surface energy. Subsequently, we assessed adhesion, proliferation, osteogenic differentiation, and potential immune activation of human osteoblast-like MG-63 cells cultured on these materials to estimate their osteointegration potential *in vivo*. The MG-63 cell line was selected due to its established utility as a model for osteoblast adhesion, growth, and differentiation on various implant materials, including titanium alloys [1, 16], PEEK [14], stainless steel [4], UHMWPE [26], and a-C:H films [24, 25]. Importantly, MG-63 cells can undergo osteogenic differentiation induced by surface physical and chemical properties (e.g., nanoroughness), obviating the need for exogenous osteogenic factors required for bone marrow mesenchymal stem cells [23].

2. MATERIALS AND METHODS

2.1. Preparation and characterization of material samples

Surface treatments and their combinations were applied to materials commonly used in orthopedic, dental, and spine surgeries (**Table 1**). Samples were cylindrical discs (2.4 or 2.9 cm diameter, 2 mm thick). Modifications included sandblasting with glass beads (0.1–0.2 mm diameter) or polishing with a buffing disk, followed by coating with a-C:H via Physical Vapor Deposition (PVD) at Prospon s.r.o., Kladno, Czech Republic.

Surface roughness was assessed on two scales. Micrometer-scale roughness (R_a, arithmetic mean of the deviations of a surface profile from its mean line) was measured using a stylus profilometer (SF 200, Planer Industrial) from 5 mm scans. Nanometer-scale roughness (R_q, root mean square roughness) was determined by atomic force microscopy (AFM, Quesant Q-scope 350) in semi-contact mode, using NSC-16 silicon cantilevers (Schaefer Technologie GmbH) from 10 µm × 10 µm scans (scan rate 2 s, resolution 512 × 512 points). All values represent averages of three measurements taken from randomly selected locations on each sample [24].

The wettability of all tested materials was determined using a goniometer with the sessile drop method, employing deionized water droplets of 3 µL volume. Each water contact angle value represents an average of at least three independent measurements taken at different locations on the samples. Additionally, surface free energy and its polar and dispersive components were calculated from the contact angles of deionized water and diiodomethane (Sigma-Aldrich), according to Fowkes's theory [27].

Material	Sandblasting (S)	Polishing (P)	a-C:H	Abbreviation
1. Ti-6Al-4V alloy	+			TiAlV_S
2. Ti-6Al-4V alloy		+		TiAlV_P
3. Ti-6Al-4V alloy	+		+	TiAlV_S_aCH
4. Ti-6Al-4V alloy		+	+	TiAlV_P_aCH
5. Stainless steel AISI 316 LWM	+			AISI_S
6. Stainless steel AISI 316 LWM		+		AISI_P
7. PEEK Optima				PEEK
8. PEEK Optima		+		PEEK_P
9. UHMWPE				UHMWPE
10. UHMWPE		+		UHMWPE_P

Table 1. Materials and their surface modifications

2.2. Cell model and culture conditions

For cell cultivation, the material samples were cleaned with 70% ethanol, thoroughly rinsed with distilled and deionized water, and sterilized in an autoclave (Tuttnauer 2540 ELC; 121°C for 30 minutes). The sterilized samples were then placed into 6-well polystyrene plates (TPP, Trasadingen, Switzerland; well diameter: 3.4 cm) and seeded with human osteoblast-like MG-63 cells (European Collection of Cell Cultures, Salisbury, UK). Approximately 17,000 cells were seeded per well, which contained 6 mL of Dulbecco's Modified Eagle Medium (DMEM; Sigma-Aldrich, Cat. No. D5648) supplemented with 10% fetal bovine serum (FBS; Sebak GmbH, Aidenbach, Germany) and 40 µg/mL gentamicin (LEK, Ljubljana, Slovenia). Cells were cultured at 37°C in a humidified air atmosphere containing 5% CO_2 for 1, 3, or 8 days.

Evaluation of the cell adhesion and growth

On day 1 post-seeding, cells on the material surfaces were fixed using cold 70% ethanol and stained with two fluorescent dyes diluted in phosphate-buffered saline (PBS): Texas Red C_2-Maleimide (Molecular Probes, Invitrogen, Paisley, UK; 20 ng/mL), which labels proteins in the cell membrane and cytoplasm, and Hoechst #33342 (Sigma-Aldrich; 5 µg/mL), which stains cell nuclei. Cell number, morphology, spreading area, and distribution across the surface were assessed using images captured

with an Olympus IX51 microscope equipped with a DP70 digital camera (Olympus, Japan). For each experimental group, 18 micrographs (nine from each of two samples) were analyzed.

Cell spreading area was quantified using Atlas Software (Tescan, Brno, Czech Republic). Cells exhibiting intercellular contacts were excluded from analysis. Between 69 and 158 cells were evaluated per experimental group [17, 18, 24].

On days 3 and 8, when cell density was high and overlapping precluded accurate counting by microscopy, cells were detached enzymatically with Trypsin-EDTA solution (Sigma-Aldrich, Cat. No. T4174) in PBS for 10 minutes at 37°C. Detached cells were resuspended in culture medium and counted automatically using a Vi-CELL XR analyzer (Beckman Coulter, USA). Viability was assessed via the trypan blue exclusion test during counting. For each experimental group and time point, 3–5 samples were analyzed, with 50 measurements performed per sample (totaling 150–250 measurements).

Cell counts at days 1, 3, and 8 were expressed as population density (cells/cm²) and used to construct growth curves. Cell population doubling times (DT) between days 1 and 3, and between days 3 and 8, were calculated using the equation:

$$DT = \frac{log2(t - t_0)}{-\,log\ log\ N_{t_0}}$$

where t_o and t represent earlier and later time intervals after seeding, respectively, and N_{t_0} and N_t represent the number of cells at these intervals [15].

2.3. Immunofluorescence staining

On day 3, the cytoskeletal protein β-actin was visualized by immunofluorescence to assess its spatial distribution and organization within cells. Cells were incubated overnight at 4°C with monoclonal mouse anti-β-actin primary antibody (Sigma-Aldrich, Cat. No. A5441, clone AC-15) diluted 1:200 in PBS. After washing with PBS, cells were incubated at room temperature for 1 hour in the dark with a goat anti-mouse IgG ($F(ab')_2$ fragment) secondary antibody conjugated with Alexa Fluor® 488 (Molecular Probes, Invitrogen; Cat. No. A11017), diluted 1:1000. Subsequently, cells were washed twice with PBS, mounted under glass coverslips in Gel/Mount aqueous mounting medium (Biomeda Corporation, Foster City, CA, USA), and examined using an Olympus IX71 epifluorescence microscope equipped with a DP70 digital camera (Olympus, Japan) [17, 18, 24].

2.4. Enzyme-linked immunosorbent assay (ELISA)

The concentrations of molecular markers related to cell adhesion, osteogenic differentiation, and immune activation were measured in homogenates of MG-63 cells after 3 days of cultivation (α_v- and β_1-integrins, talin, vinculin, β-actin) or after 8 days (osteocalcin, osteopontin, and ICAM-1). Trypsinized cells were resuspended in PBS, centrifuged, then resuspended in distilled and deionized water at a concentration of 10^6 cells/mL and stored at −70°C overnight. Subsequently, cells were homogenized by ultrasonication for 40 seconds using a sonicator (UP 100 H, Dr. Hielscher GmbH, Germany).

Total protein content was measured by a modified Lowry method [28], previously adapted in our studies (e.g., [24]). Aliquots of cell homogenates containing 1–50 µg of protein in 50 µL of water were adsorbed onto 96-well Maxisorp microtiter plates (Nunc) at 4°C overnight. After washing twice with PBS (100 µL/well), nonspecific antibody-binding sites were blocked with 0.02% gelatin in PBS (100 µL/well, 60 min), followed by treatment with 1% Tween-20 (Sigma-Aldrich, Cat. No. P1379; 100 µL/well, 20 min).

Primary antibodies (see **Table 2**), diluted in PBS, were applied for 60 minutes at room temperature (50 µL/well). Goat anti-mouse $F(ab')_2$ IgG (Sigma-Aldrich, Cat. No. A3682; 1:1000 dilution in PBS) was used as the secondary antibody following mouse monoclonal primaries, and goat anti-rabbit IgG (Sigma-Aldrich, Cat. No. A9169; 1:5000 dilution) was used following rabbit polyclonal antibodies or antiserum. Both secondary antibodies were peroxidase-conjugated and incubated for 45 minutes at room temperature (50 µL/well).

After double washing with PBS, the orthophenylenediamine reaction was performed (Sigma-Aldrich, Cat. No. P1526; 2.76 mM concentration) with 0.05% H_2O_2 in 0.1 M phosphate buffer (pH 6.0) in the

dark (100 µL/well). The reaction was stopped after 10–30 minutes by adding 50 µL/well of 2 M H_2SO_4. Absorbance was measured at 490 and 690 nm using a Versa Max Microplate Reader (Molecular Devices Corporation, Sunnyvale, CA, USA). Absorbance values from cells grown on test samples were expressed as percentages relative to control cultures grown on standard polystyrene wells.

Antibody	Company	Cat. No., Clone	Dilution
Monoclonal mouse antihuman β_1-integrin	Chemicon	MAB 1981, LM534	1:200
Monoclonal mouse anti-chicken talin	Sigma-Aldrich	T3287, 8D4	1:200
Monoclonal mouse anti-human vinculin	Sigma-Aldrich	V9131, hVIN-1	1:400
Monoclonal mouse anti-β-actin	Sigma-Aldrich	A5441, AC-15	1:200
Monoclonal mouse anti-human ICAM-1	Exbio s.r.o., CR	11-228, MEM 111	1:200
Polyclonal rabbit anti-human α_v-integrin	Chemicon	AB 1930	1:400 to 1:800
Polyclonal rabbit anti-human osteopontin	Alexis	ALX-210-309	1:500
Rabbit anti-human osteocalcin (1-49) purified antiserum IgG	Bachem Group, Peninsula Laboratories Inc., CA, USA	T-4743.0400	1:500

Table 2. Primary antibodies used for ELISA

2.5. Statistical analysis

Surface roughness parameters (R_a and R_q) and water contact angle values are presented as mean ± standard deviation (SD). Quantitative biological data (cell counts, spreading areas, protein concentrations) are expressed as mean ± standard error of the mean (SEM). Statistical significance among experimental groups was assessed using one-way analysis of variance (ANOVA) followed by the Student–Newman–Keuls post hoc test (SigmaStat for Windows, version 3.5, Systat Software, Inc.). P-values ≤ 0.05 were considered statistically significant.

3. RESULTS

3.1. Physical and chemical properties of the material surface

The surface roughness, quantified by the R_a parameter, was generally low across all samples. Unmodified or sandblasted samples exhibited submicrometer-scale roughness (0.1 to 1 µm), whereas polished samples had mostly nanoscale roughness (<100 nm).

The R_a parameter, which indicates the height or depth of surface irregularities, was lower on metallic samples modified by sandblasting or sandblasting plus a-C:H coating (347 ± 9 nm to 600 ± 16 nm) than on unmodified polymeric samples (977 ± 45 nm to 1790 ± 43 nm), especially for UHMWPE. Polishing markedly reduced R_a values: on polished metallic samples and PEEK, R_a ranged from 57 ± 26 to 80 ± 22 nm (nanoscale roughness), while polished UHMWPE had an R_a of 250 ± 33 nm, remaining within submicrometer roughness (**Fig. 1A**). Surface roughness on polystyrene wells was negligible (R_a = 0.51 nm).

Similar trends were observed for root mean square (RMS) roughness (R_q), measured by AFM on metallic and a-C:H-coated samples, with a significant roughness decrease after polishing (**Fig. 1B**). AFM scans (**Fig. 2**) illustrate the globular features formed by the a-C:H film on coated samples.

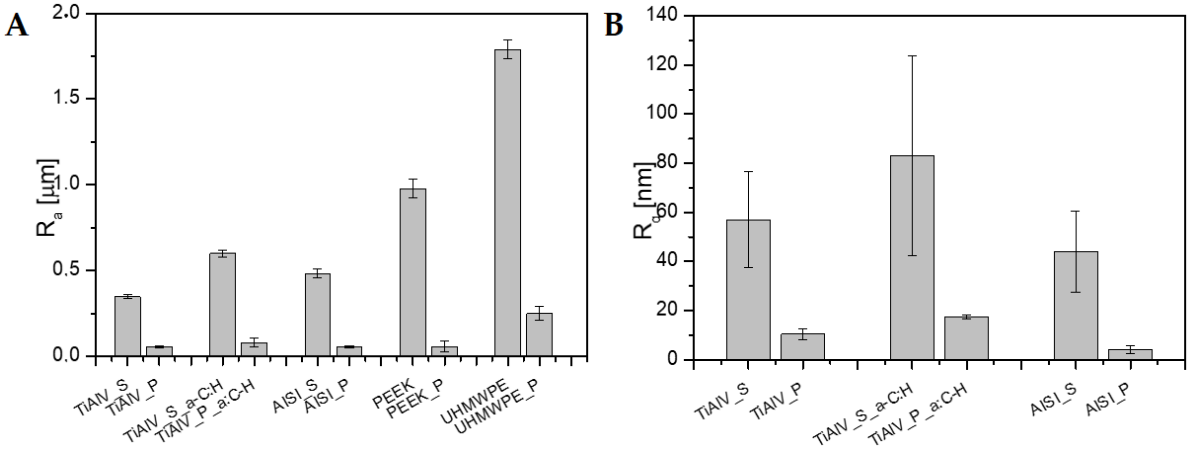

Fig. 1. The surface roughness of metallic and polymeric samples with various surface modifications listed in Table 1. **A**. R_a roughness determined by stylus profilometry. **B**. R_q nano-roughness estimated from AFM scans (it was not possible to determine surface roughness of PEEK and UHMWPE samples due to the limited z-scale range of the employed AFM). Mean ± S.D. from 3 measurements for each parameter and experimental group.

Water drop contact angles, inversely correlated with wettability, ranged from 58° to 87° (**Fig. 3A**). The a-C:H-coated Ti-6Al-4V samples showed the lowest contact angles and highest wettability, consistent with their highest polar surface energy (**Fig. 3B**). UHMWPE samples exhibited nearly hydrophobic behavior (water contact angles of 87° ± 4° in unmodified and 82° ± 5° in polished samples). Polishing effects on wettability varied: slight increases were observed in Ti-6Al-4V, AISI, and UHMWPE samples, slight decreases in PEEK, and no significant change in a-C:H-coated Ti-6Al-4V samples. For comparison, standard cell culture polystyrene wells had a contact angle of 60° ± 4°.

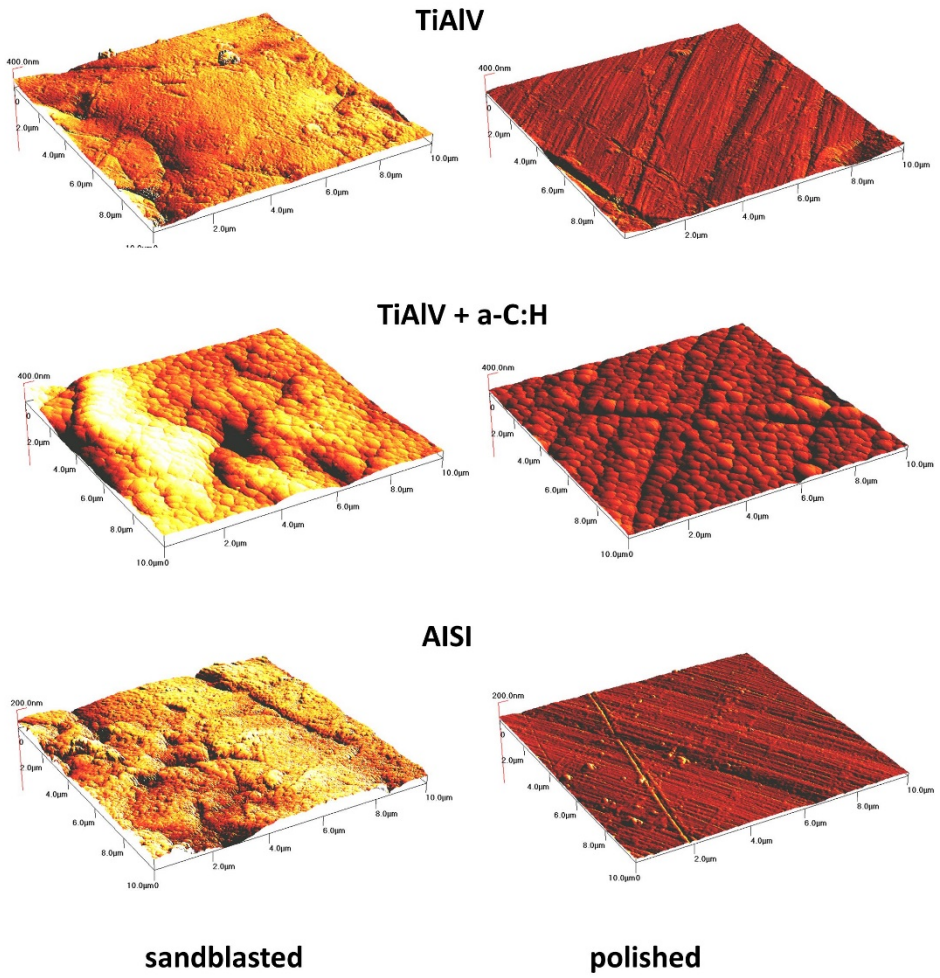

Fig. 2. Examples of 10 µm x 10 µm AFM scans of sandblasted (left) and polished (right) TiAlV, TiAlV + a-C:H and AISI samples. The Z-scale is 400 nm for TiAlV and TiAlV + a-C:H samples and 200 nm for AISI samples.

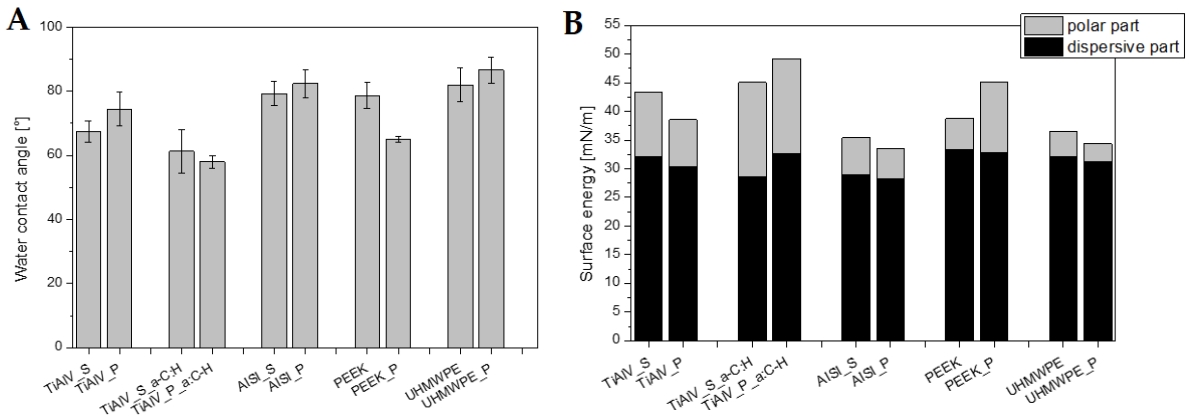

Fig. 3. Surface wettability (**A**) and polar and dispersive parts of surface energy (**B**) of metallic and polymeric samples with various surface modifications, as listed in Table 1. A: Mean ± S.D. from 3 measurements for each parameter and experimental group.

3.2. Cell adhesion and growth

On day 1 post-seeding, the number of cells adhering to all materials was lower (19,000 ± 6,300 to 49,000 ± 12,000 cells/cm²) than to polystyrene control wells (61,000 ± 17,000 cells/cm²), except for the Ti-6Al-4V sample treated by sandblasting and coated with a-C:H, where cell numbers were comparable to polystyrene. Moreover, TiAlV_S_aCH samples supported significantly higher cell adhesion than other metallic and polymeric samples. Unmodified UHMWPE showed significantly fewer adhered cells compared to others, but polishing significantly increased cell adhesion. Polishing had no significant effect on initial cell adhesion for other materials, except for a-C:H-coated samples, where polishing significantly decreased cell numbers (**Fig. 4A**).

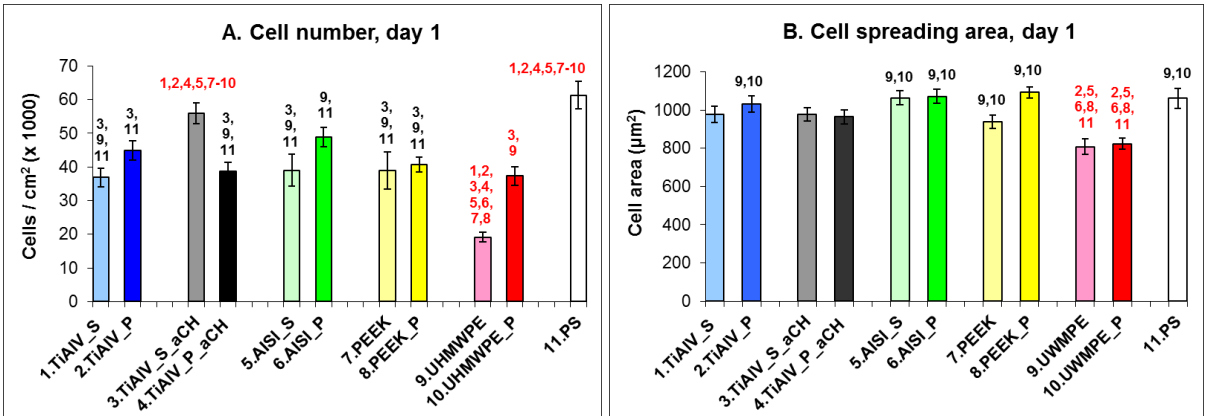

Fig. 4. The number (**A**) and spreading area (**B**) of human osteoblast-like MG-63 cells on day 1 after seeding on metallic and polymeric samples with various surface modifications listed in Table 1, and in control polystyrene (PS) wells. Mean ± S.E.M. from 18 measurements (A) or from 69-158 cells (B) for each experimental group. ANOVA, Student-Newman-Keuls Method. Statistical significance: $p \leq 0.05$ compared to the groups indicated by their numbers above the columns.

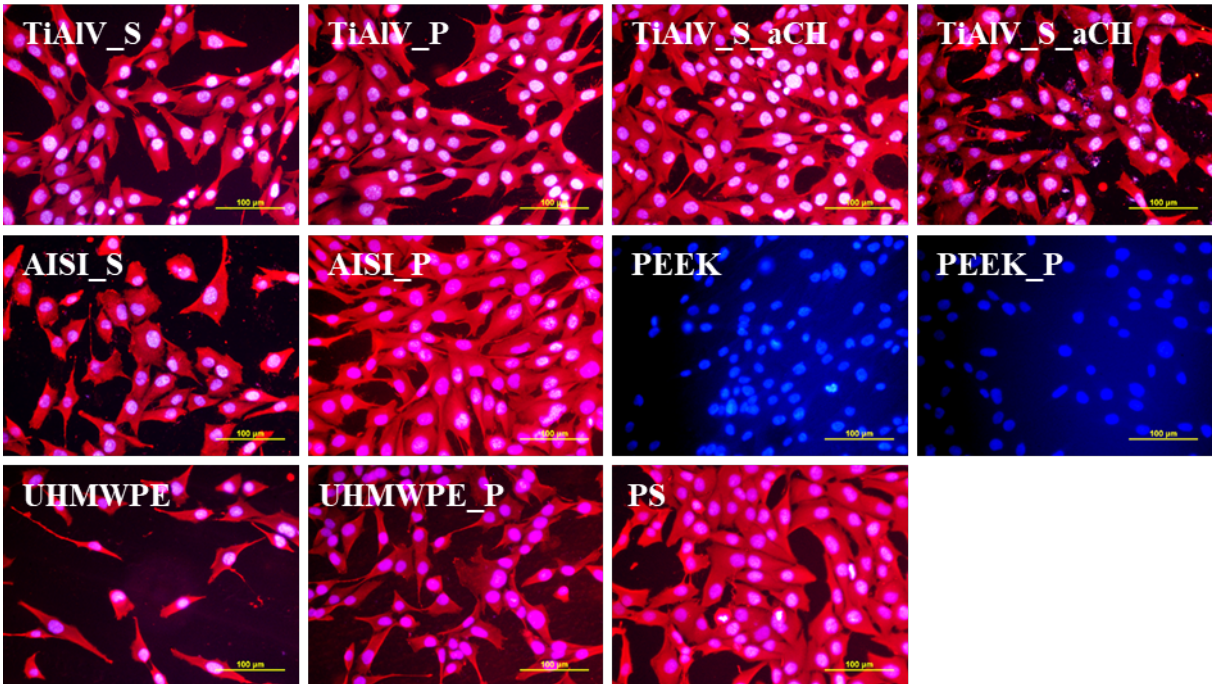

Fig. 5. Morphology and distribution of human osteoblast-like MG-63 cells on metallic and polymeric samples with various surface modifications listed in Table 1, and in control polystyrene (PS) wells. The cells were stained with Texas Red C_2-Maleimide (red fluorescence) and Hoechst #33342 (blue/pink fluorescence). The PEEK and PEEK_P images were made using a blue fluorescence filter only due to the red autofluorescence of PEEK. Olympus IX 51 microscope, obj. 20, DP 70 digital camera, bar = 100 µm.

The cell spreading area was the smallest on the UHMWPE samples. On the other samples, the cell spreading areas were similar to the values on polystyrene (**Fig. 4B**). On all tested samples, the cells were polygonal or spindle-shaped, indicating good cell-material interaction. They were also homogeneously distributed on the material surface (**Fig. 5**). PEEK samples showed high red autofluorescence under a conventional microscope; thus, cell spreading area and morphology were evaluated using confocal microscope images, which allowed for the removal of autofluorescence (**Fig. 6**).

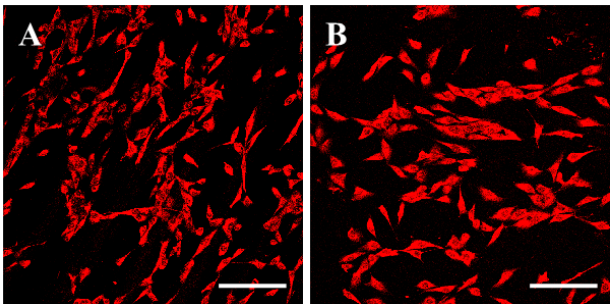

Fig. 6. Human osteoblast-like MG-63 cells on day 1 after seeding on non-modified (**A**) and polished (**B**) PEEK. The cells were stained with Texas Red C_2-Maleimide (red fluorescence) and Hoechst #33342. Only the Texas Red C_2-Maleimide fluorescence is visible. Confocal microscope: Leica SP2; objective: 10x; scale bar = 200 µm.

From day 1 to day 3 after seeding, the cells on all the tested samples proliferated with a doubling time between 30 and 56 hours and increased in number (**Table 3, Fig. 7A**). However, the cells on the polished UHMWPE did not proliferate, and the number of cells on day 3 was similar to the number on day 1 (36,000 ± 2,000 cells/cm²). This stagnation is also clearly visible in the growth curves **(Fig. 8)**. The cell number was also very low on unmodified UHMWPE samples (50,000 ± 3,000 cells/cm²), probably due to the low number of cells that initially adhered, as their doubling time (34 hours) was within the range found in cells on the other samples (**Table 3, Fig. 7A**).

Material /DT	TiAlV_S	TiAlV_P	TiAlV_S_aCH	TiAlV_P_aCH	AISI_S	AISI_P	PEEK	PEEK_P	UHMWPE	UHMWPE_P	PS
DT 1-3 (h)	33	56	41	30	43	39	42	42	34	n.a.	51
DT 3-8 (h)	54	63	63	55	57	67	47	53	43	64	74

Table 3. Doubling time (DT, hours) of human osteoblast-like MG-63 cells between days 1 and 3 (**DT 1-3**) and between days 3 and 8 (**DT 3-8**) after seeding on metallic and polymeric samples with various surface modifications listed in Table 1, and in control polystyrene (PS) wells.

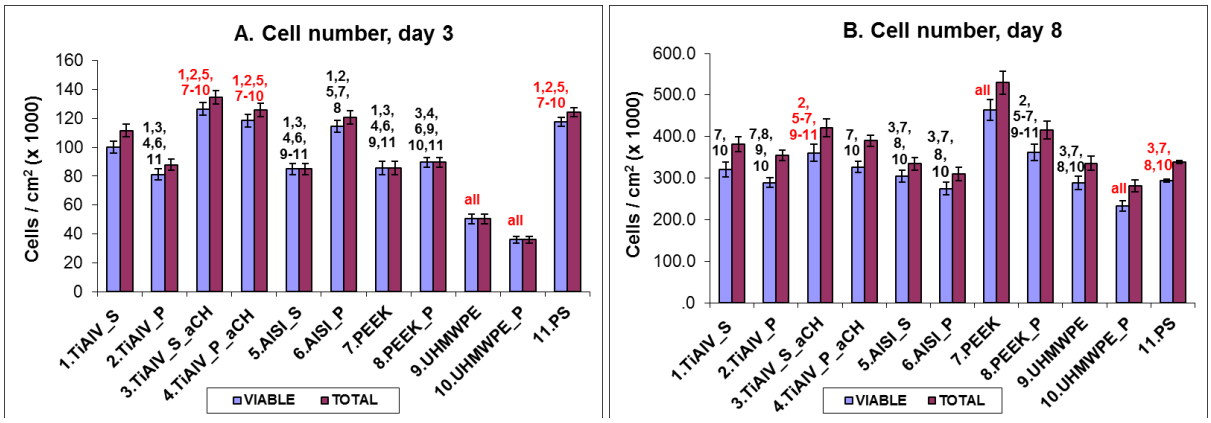

Fig. 7. The number of human osteoblast-like MG-63 cells on day 3 (**A**) and on day 8 (**B**) after seeding on metallic and polymeric samples with various surface modifications listed in Table 1, and in control polystyrene (PS) wells. Mean ± S.E.M. from 150-250 measurements obtained from 3-5 samples for each experimental group and time interval. ANOVA, Student-Newman-Keuls Method. Statistical significance: $p \leq 0.05$ compared to the groups indicated by their numbers above the columns.

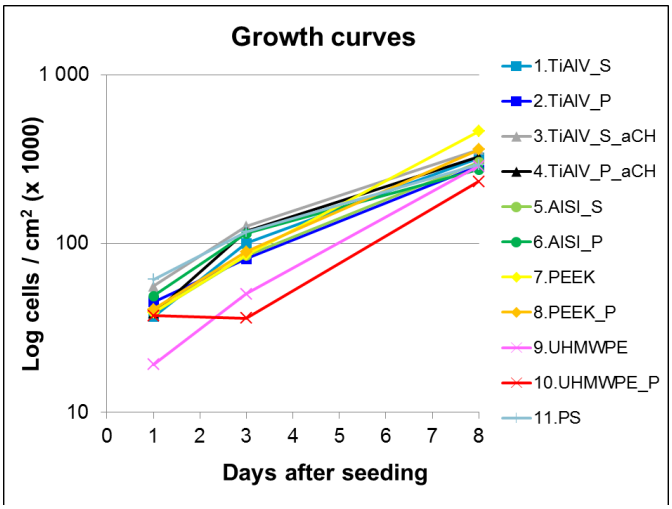

Fig. 8. Growth dynamics of human osteoblast-like MG-63 cells from day 1 to day 8 after seeding on metallic and polymeric samples with various surface modifications listed in Table 1, and in control polystyrene (PS) wells.

Immunofluorescence staining performed on day 3 showed that the cells on all of the tested samples, including the UHMWPE sample, were well-spread, mostly polygonal, and had a well-developed actin cytoskeleton (**Fig. 9**).

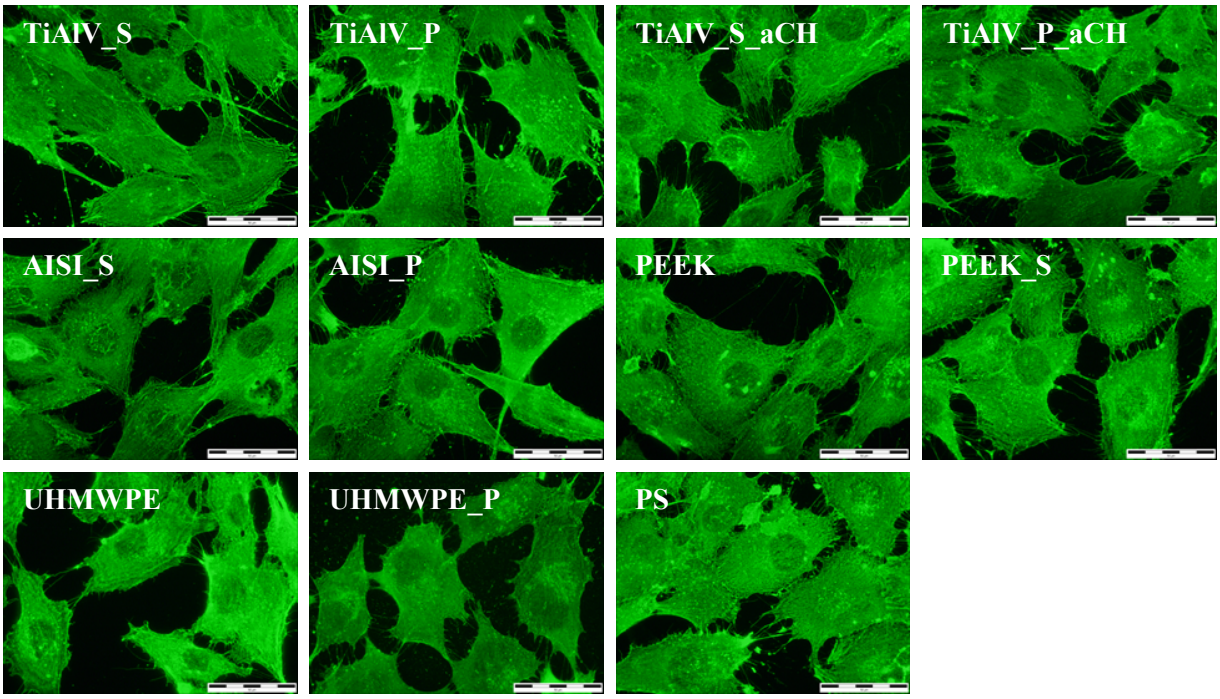

Fig. 9. Immunofluorescence staining of β-actin in human osteoblast-like MG-63 cells on day 3 after seeding on metallic and polymeric samples with various surface modifications listed in Table 1, and in control polystyrene (PS) wells. Olympus IX 71 microscope, obj. 100×, DP 70 digital camera, bar = 50 μm.

On day 8 after seeding, cell viability remained high, though lower than on day 3 (81-91% vs. 90-100%). This may be because the cells reached confluence and entered the stationary phase of growth, which is associated with increased cell death compared to the exponential phase. The cell numbers in almost all samples were similar to those in the control polystyrene wells (294,000 ± 3,000 cells/cm^2). The cell numbers exceeded the values in polystyrene wells on sandblasted and a-C:H-coated Ti-6Al-4V (361,000 ± 21,000 cells/cm^2), as well as on non-modified and polished PEEK (464,000 ± 25,000 cells/cm^2 and 362,000 ± 19,000 cells/cm^2, respectively). However, on polished UHMWPE, the cell number (233,000 ± 13,000) remained the lowest among all tested groups (**Fig. 7B**), although these cells proliferated with similar growth dynamics to the other samples (**Table 3, Fig. 8**).

3.3. Concentration of molecular markers of cell adhesion, differentiation and immune activation

ELISA analysis demonstrated that materials exhibiting the highest cell population densities also showed elevated levels of molecules involved in cell adhesion (α_v- and β_1-integrins, vinculin, talin) and osteogenic differentiation (osteocalcin and osteopontin). These materials included AISI stainless steel, polished and a-C:H-coated Ti-6Al-4V, and polished PEEK.

Specifically, the concentration of α_v-integrins —receptors for vitronectin and fibronectin, which adsorb spontaneously from serum—was significantly higher on polished AISI stainless steel than on most other samples, except UHMWPE and polystyrene controls (**Fig. 10A**). Beta$_1$-integrins, primarily receptors for fibronectin and collagen (produced and deposited by cells), were most abundant on sandblasted and a-C:H-coated Ti-6Al-4V, with relatively high levels on polished AISI stainless steel and polished PEEK (**Fig. 10B**).

Vinculin, an integrin-associated protein stabilizing focal adhesion plaques, peaked on polished AISI stainless steel (**Fig. 10C**). In contrast, polished PEEK exhibited relatively low vinculin but a high concentration of talin, another focal adhesion plaque protein (**Fig. 10D**).

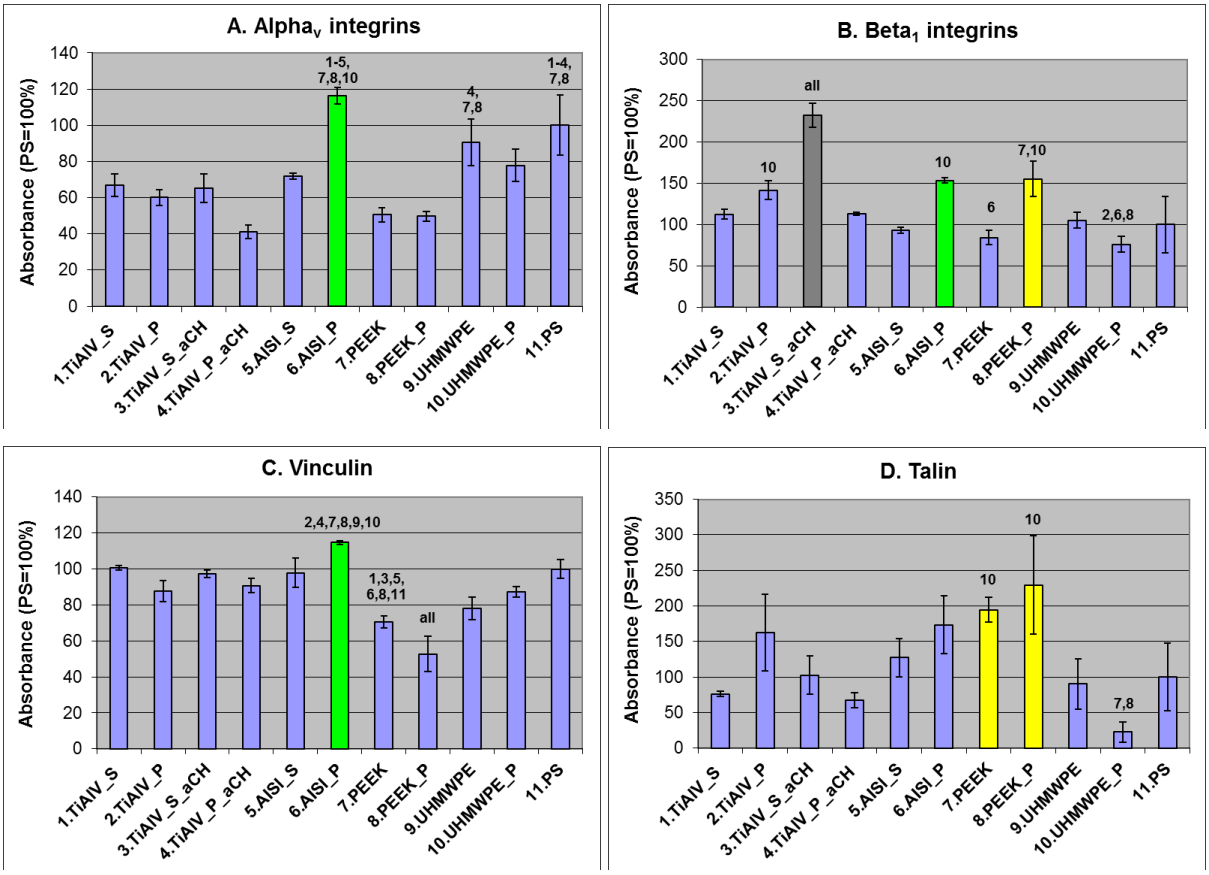

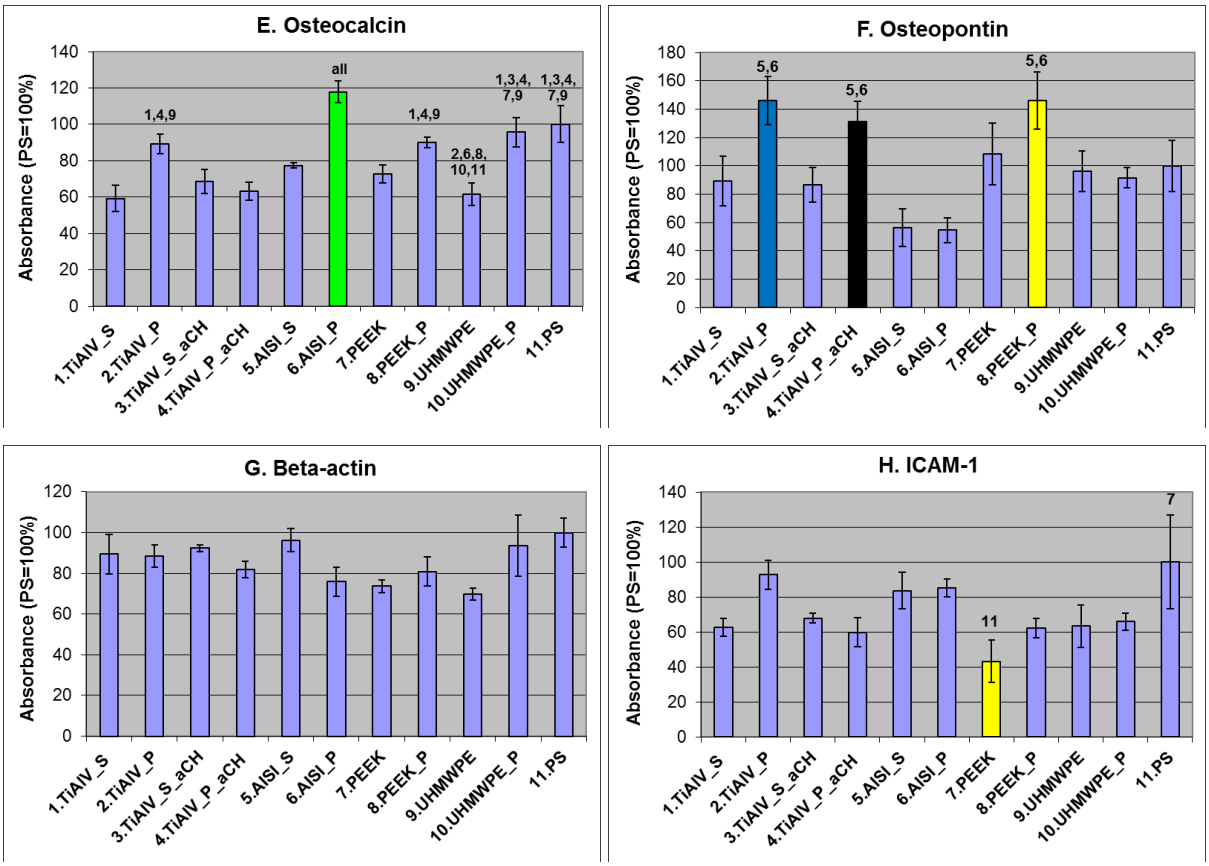

Fig. 10. Concentration of molecular markers of cell adhesion (**A-D**), osteogenic cell differentiation (**E, F**), cytoskeletal protein β-actin (**G**) and ICAM-1, a marker of cell immune activation (**H**) in cells on day 3 (A-D, G) or on day 8 (E, F, H) after seeding on materials with various surface modifications listed in Table 1. Measured by ELISA per mg of protein in cell homogenates. Absorbance values are expressed in % of values obtained from standard cell culture wells. Mean ± S.E.M. from 3 experiments performed in triplicate (in total 9 measurements for each experimental group). ANOVA, Student-Newman-Keuls Method. Statistical significance: $p \leq 0.05$ compared to the groups indicated by their numbers above the columns.

Osteocalcin, a key marker of osteogenic differentiation, was most concentrated in cells on polished AISI samples (**Fig. 10E**), while osteopontin levels were relatively high on polished AISI, polished Ti-6Al-4V, and polished PEEK (**Fig. 10F**). Beta-actin concentrations were similar across all samples, consistent with its role as a ubiquitous cytoskeletal protein arranged in filament bundles throughout the cytoplasm (**Fig. 9** and **Fig. 10G**).

The immune activation marker ICAM-1 was similarly expressed in cells on all materials and polystyrene controls, with slightly lower levels on natural PEEK (**Fig. 10H**). Although ICAM-1 facilitates binding of inflammatory cells and osteoclast precursors, promoting bone resorption, some studies also regard ICAM-1 as indicative of biomaterial biocompatibility and osteoblast adhesion. Given its potential to stimulate osteoclastic precursor differentiation and tumor cell migration, the relatively low ICAM-1 levels in MG-63 cells across all materials suggest a favorable immune profile.

4. DISCUSSION

All materials tested in this study promoted adhesion, spreading, actin cytoskeleton formation, and proliferation of human osteoblast-like MG-63 cells, although the degree of support varied among them. On day 1, the highest initial cell adhesion was observed on sandblasted Ti-6Al-4V coated with a-C:H

(TiAlV_S_aCH), which also exhibited the highest concentration of β_1-integrin adhesion receptors—key mediators of fibronectin and collagen binding—indicating strong cell-material interactions. Signaling via β_1-integrins, particularly $\alpha_2\beta_1$, is crucial for osteogenic differentiation [1]. Surprisingly, the highest levels of osteogenic markers osteopontin and osteocalcin were found not on TiAlV_S_aCH but on polished materials such as AISI stainless steel (osteocalcin) and TiAlV_P, TiAlV_P_aCH, and polished PEEK (osteopontin), likely due to their favorable nanoroughness and moderate wettability (contact angles 58.0 ± 2.0° to 82.3 ± 4.5°), which are known to enhance osteogenic differentiation [2, 3, 23].

By day 3, cell density remained highest on TiAlV_S_aCH and TiAlV_P_aCH samples, whereas samples treated only by sandblasting or polishing showed significantly lower cell numbers. This suggests that the a-C:H coating plays a more vital role than sandblasting or polishing alone in promoting cell adhesion on Ti-6Al-4V. Although a-C:H coatings, including diamond-like carbon (DLC), are typically considered bioinert [24,29], their moderate wettability and nanoscale roughness—properties confirmed in our coatings—can enhance cell adhesion and growth, consistent with findings by Lopez-Santos *et al*. [25]. These coatings also improve surface chemical stability and mechanical properties, reduce the release of cytotoxic ions and particles, and decrease friction and wear in orthopedic applications [25, 30, 31]. Additionally, a-C:H films have demonstrated utility in blood-contacting devices due to their anti-thrombotic properties and have been used to create antimicrobial and anti-protein adsorption surfaces [25, 32–35].

The wettability and surface roughness of a-C:H films can be modulated by the deposition method (e.g., plasma-enhanced chemical vapor deposition, ion beam deposition, pulsed laser ablation, or pulsed reactive magnetron processes) and the settings of these procedures (e.g., power density, voltage, deposition time, and the use of methane or deuterated methane) [25, 36]. Different approaches to a-C:H deposition can result in varying degrees of film oxidation. The presence of oxygen in the form of oxygen-containing chemical functional groups on the a-C:H surface increases wettability and polarity, consequently enhancing cell adhesion and growth [21, 25].

Other atoms that can be incorporated into a-C:H films to modify their physical and chemical properties, as well as the adhesion and growth of osteogenic and other cell types, include Ti [15, 24, 29], B [25], N [32], or Si [36]. Even potentially cytotoxic elements such as Ag or Cu, which were originally incorporated to enhance the antimicrobial, mechanical, tribological, and corrosion properties of a-C:H, can promote the adhesion and growth of osteogenic cells or exhibit an angiogenic effect [33, 34]. Factors such as hydrogen content, sp^2/sp^3 carbon bond ratios, and film structure (e.g. the I^D/I^G ratio, which is a key indicator of structural disorder and defects in carbon-based materials as determined by Raman spectroscopy) can also influence MG-63 cell proliferation [25, 36].

UHMWPE samples showed the lowest initial cell adhesion and spreading on day 1, with persistently low cell numbers at later time points, reflecting the material's hydrophobicity (contact angle near 90°) and typical use in articular surfaces where cell adhesion is undesirable to prevent fibrotic encapsulation, arthrofibrosis and reduced mobility [6,7,30,31]. On hydrophobic surfaces, key adhesion proteins adsorb in denatured conformations, reducing integrin binding and cell adhesion [21]. Polishing UHMWPE improved initial adhesion by inducing nanoscale surface roughness, which can restore favorable protein conformations for adhesion receptor recognition, similar to wettable surfaces [21]. Despite this, day 8 cell densities on polished UHMWPE remained the lowest overall. Interestingly, cells on polished UHMWPE had relatively high osteocalcin levels, likely due to reduced proliferation allowing differentiation to proceed, a phenomenon also observed on microscale rough surfaces that inhibit proliferation but promote osteogenesis [16, 22].

Polished stainless steel (AISI_P) supported relatively high cell numbers and spreading despite its hydrophobic nature, likely due to compensatory nanoscale roughness. Cells on AISI_P exhibited increased α_v integrin levels, receptors for vitronectin, which preferentially adsorbs on nanostructured surfaces [21]. Alpha$_v$-integrin signaling supports osteogenic differentiation [38, 39], consistent with the elevated osteocalcin, β_1-integrin, and vinculin concentrations observed. Vinculin stabilizes focal adhesions and is also associated with osteogenic cell differentiation [1, 10, 39].

Unmodified PEEK supported the highest cell density by day 8, despite being considered bioinert and generally less conducive to osteogenic cell adhesion, growth and differentiation than titanium alloys [14, 16]. Some reports have shown comparable or higher osteoblast proliferation on PEEK versus titanium [16, 40]. Polishing in our study increased osteocalcin and osteopontin levels on PEEK, likely due to enhanced nanoroughness and wettability. A wide variety of modifications can improve the bioactivity and osseointegration of PEEK. Recent modifications include plasma activation followed by coating with gelatin [13], titanium oxide and hyaluronic acid [14], strontium decoration [41], especially in combination with bioactive glass [11], coating or blending the polymer with phosphate-based minerals [9], functionalization with cell-adhesive peptides [19], or bone morphogenetic proteins [20]. Another method is coating the polymer with a nanostructured TiNb layer, as demonstrated in our recent study [42]. Due to its radiolucency and bone-like mechanical properties, PEEK remains a promising alternative to metallic implants [5].

Finally, ICAM-1 expression, an immune activation marker, was low and comparable across all materials and control polystyrene, with the lowest levels on PEEK. While ICAM-1 is involved in osteoblast adhesion and is even considered a late osteogenic marker [48, 49], elevated expression is associated with inflammatory bone diseases and may promote osteoclast activity and tumor cell migration [43–50]. Therefore, the low ICAM-1 levels observed here indicate minimal immune activation and favorable biocompatibility.

5. CONCLUSIONS

All tested materials—Ti-6Al-4V, stainless steel AISI 316 LWM, PEEK, and UHMWPE—and surface modifications including sandblasting, polishing, and a-C:H coating supported MG-63 cell adhesion, spreading, actin cytoskeleton assembly, viability, growth, and osteogenic differentiation to varying degrees. None of the materials or modifications significantly activated the immune response, as measured by ICAM-1 expression. The most favorable outcomes were observed with sandblasted Ti-6Al-4V coated with a-C:H, polished stainless steel, and polished PEEK. These materials exhibited the highest cell densities and elevated concentrations of adhesion molecules (β_1-integrins on sandblasted Ti-6Al-4V coated with a-C:H, α_v-integrins and vinculin on polished stainless steel, and talin on polished PEEK) and osteogenic markers (osteocalcin on polished stainless steel, osteopontin on polished PEEK). These findings identify these materials and modifications as the most suitable candidates for bone implant applications.

ACKNOWLEDGMENTS

This study was supported by the Project "Materials and technologies for sustainable development" (MATUR) No. CZ.02.01.01/00/22_008/0004631 of the Ministry of Education, Youth and Sports of the Czech Republic, co-funded by the European Union, and by the Praemium Academiae grant (No. AP2202) of the Czech Academy of Sciences.

According to Open Science principles, raw data can be found at the following link: **10.5281/zenodo.16524610**

REFERENCES

1. Olivares-Navarrete R, Rodil SE, Hyzy SL, Dunn GR, Almaguer-Flores A, Schwartz Z, Boyan BD 2015, "Role of integrin subunits in mesenchymal stem cell differentiation and osteoblast maturation on graphitic carbon-coated microstructured surfaces", *Biomaterials*, vol. 51, pp. 69-79. doi: 10.1016/j.biomaterials.2015.01.035.
2. Boyan BD, Lotz EM, Schwartz Z 2017, "Roughness and hydrophilicity as osteogenic biomimetic surface properties", *Tissue Engineering Part A*, vol. 23, no. 23-24, pp. 1479-1489. doi: 10.1089/ten.TEA.2017.0048.

3. Calciolari E, Hamlet S, Ivanovski S, Donos N 2018, "Pro-osteogenic properties of hydrophilic and hydrophobic titanium surfaces: Crosstalk between signalling pathways in *in vivo* models", *J Periodontal Research*, vol. 53, no 4, pp. 598-609. doi: 10.1111/jre.12550.
4. Gatto ML, Cerqueni G, Groppo R, Santecchia E, Tognoli E, Defanti S, Mattioli-Belmonte M, Mengucci P 2023, "Improved biomechanical behavior of 316L graded scaffolds for bone tissue regeneration produced by laser powder bed fusion", *Journal of the Mechanical Behavior of Biomedical Materials*, vol. 144, article no. 105989. doi: 10.1016/j.jmbbm.2023.105989
5. Sun Y, Ma S, Shi Y, Chen M, Lan Y, Hu L, Yang X 2025, "Overcoming biological inertness: multifaceted strategies to optimize PEEK bioactivity for interdisciplinary clinical applications", *Biomaterials Science*, vol. 13, no. 12, pp. 3106-3122. doi: 10.1039/d4bm01693a.
6. Rodrigues MM, Fontoura CP, Garcia CSC, Martins ST, Henriques JAP, Figueroa CA, Roesch-Ely M, Aguzzoli C 2019, "Investigation of plasma treatment on UHMWPE surfaces: Impact on physicochemical properties, sterilization and fibroblastic adhesion", *Materials Science & Engineering C-Materials for Biological Applications*, vol. 102, pp. 264-275. doi: 10.1016/j.msec.2019.04.048.
7. Hasegawa M, Tone S, Naito Y, Sudo A 2023, "Ultra-High-Molecular-Weight Polyethylene in Hip and Knee Arthroplasties", *Materials (Basel)*, vol. 16, no. 6, article no. 2140. doi: 10.3390/ma16062140.
8. Hadjicharalambous C, Buyakov A, Buyakova S, Kulkov S, Chatzinikolaidou M 2015, "Porous alumina, zirconia and alumina/zirconia for bone repair: fabrication, mechanical and *in vitro* biological response", *Biomedical Materials*, vol. 10, no. 2, article no. 025012. doi: 10.1088/1748-6041/10/2/025012.
9. Martínková M, Zárybnická L, Viani A, Killinger M, Mácová P, Sedláček T, Oralová V, Klepárník K, Humpolíček P 2024, "Polyetheretherketone bioactivity induced by farringtonite", *Scientific Reports*, vol. 14, no. 1, article no. 12186. doi: 10.1038/s41598-024-61941-3.
10. Ojansivu M, Hyväri L, Kellomäki M, Hupa L, Vanhatupa S, Miettinen S 2018, "Bioactive glass induced osteogenic differentiation of human adipose stem cells is dependent on cell attachment mechanism and mitogen-activated protein kinases", *European Cells and Materials*, vol. 35, pp. 54-72. doi: 10.22203/eCM.v035a05.
11. Xu Z, Miao L, Meng X, Sui J, Chen M, Zheng Z, Huo S, Liu S, Zhang H 2024, "Strontium-doped bioactive glass-functionalized polyetheretherketone enhances osseointegration by facilitating cell adhesion", *Colloids and Surfaces B: Biointerfaces*, vol. 241, article no. 114042. doi: 10.1016/j.colsurfb.2024.114042.
12. Bacakova L, Filova E, Liskova J, Kopova I, Vandrovcova M, Havlikova J 2016, "Nanostructured materials as substrates for the adhesion, growth, and osteogenic differentiation of bone cells", in: *Nanobiomaterials in Hard Tissue Engineering. Applications of Nanobiomaterials*. Ed. A. M. Grumezescu, Elsevier Inc., William Andrew Publishing, Oxford, Cambridge, vol. 4, chapter 4, pp. 103-153. ISBN 978-0-323-42862-0.
13. Mehdizadeh Omrani M, Kumar H, Mohamed MGA, Golovin K, S Milani A, Hadjizadeh A, Kim K 2021, "Polyether ether ketone surface modification with plasma and gelatin for enhancing cell attachment", *Journal of Biomedical Materials Research Part B: Applied Biomaterials*, vol. 109, no. 5, pp. 622-629. doi: 10.1002/jbm.b.34726.
14. Abdulghfor MA, Mahmood MK, Noori ZF, Kurda HA, Qadir BH, Othman KS, Fatih MT, Amin S, Mahmood NK 2025, "Coating polyetheretherketone implant surface with titanium oxide nanoparticles and hyaluronic acid: An *in vitro* study", *Cureus*, vol. 17, no. 1, article no. e77383. doi: 10.7759/cureus.77383.

15. Bacáková L, Starý V, Kofronová O, Lisá V 2001, "Polishing and coating carbon fiber-reinforced carbon composites with a carbon-titanium layer enhances adhesion and growth of osteoblast-like MG63 cells and vascular smooth muscle cells *in vitro*", *Journal of Biomedical Materials Research*, vol. 54, no. 4, pp. 567-78.
16. Olivares-Navarrete R, Gittens RA, Schneider JM, Hyzy SL, Haithcock DA, Ullrich PF, Schwartz Z, Boyan BD 2012, "Osteoblasts exhibit a more differentiated phenotype and increased bone morphogenetic protein production on titanium alloy substrates than on poly-ether-ether-ketone", *The Spine Journal*, vol. 12, no. 3, pp. 265-72. doi: 10.1016/j.spinee.2012.02.002.
17. Havlikova J, Strasky J, Vandrovcova M, Harcuba P, Mhaede M, Janecek M, Bacakova L 2014, "Innovative surface modification of Ti-6Al-4V alloy with a positive effect on osteoblast proliferation and fatigue performance", *Materials Science & Engineering C-Materials for Biological Applications*, vol. 39, pp. 371-379. doi: 10.1016/j.msec.2014.03.024.
18. Gabor R, Doubkova M, Gorosova S, Malanik K, Vandrovcova M, Cvrcek L, Drobikova K, Mamulova Kutlakova K, Bacakova L 2020, "Preparation of highly wettable coatings on Ti-6Al-4V ELI alloy for traumatological implants using micro-arc oxidation in an alkaline electrolyte", *Scientific Reports*, vol. 10, no. 1, article no. 19780. doi: 10.1038/s41598-020-76448-w
19. Cassari L, Zamuner A, Messina GML, Marsotto M, Chen H, Gonnella G, Coward T, Battocchio C, Huang J, Iucci G, Marletta G, Di Silvio L, Dettin M 2023, "Bioactive PEEK: Surface enrichment of vitronectin-derived adhesive peptides", *Biomolecules*, vol. 13, no. 2, article no. 246. doi: 10.3390/biom13020246.
20. Cassari L, Zamuner A, Messina GML, Marsotto M, Chang HC, Coward T, Battocchio C, Iucci G, Marletta G, Di Silvio L, Dettin M 2023, "Strategies for the covalent anchoring of a BMP-2-mimetic peptide to PEEK surface for bone tissue engineering", *Materials (Basel)*, vol. 16, no. 10, article no. 3869. doi: 10.3390/ma16103869.
21. Bacakova L, Filova E, Parizek M, Ruml T, Svorcik V 2011, "Modulation of cell adhesion, proliferation and differentiation on materials designed for body implants", *Biotechnology Advances*, vol. 29, no. 6, pp. 739-767. doi: 10.1016/j.biotechadv.2011.06.004.
22. Lee EM, Smith K, Gall K, Boyan BD, Schwartz Z 2016, "Change in surface roughness by dynamic shape-memory acrylate networks enhances osteoblast differentiation", *Biomaterials*, vol. 110, pp. 34-44. doi: 10.1016/j.biomaterials.2016.08.004.
23. Gittens RA, Olivares-Navarrete R, Cheng A, Anderson DM, McLachlan T, Stephan I, Geis-Gerstorfer J, Sandhage KH, Fedorov AG, Rupp F, Boyan BD, Tannenbaum R, Schwartz Z 2013, "The roles of titanium surface micro/nanotopography and wettability on the differential response of human osteoblast lineage cells", *Acta Biomaterialia*, vol. 9, no. 4, pp. 6268-6277. doi: 10.1016/j.actbio.2012.12.002.
24. Grinevich A, Bacakova L, Choukourov A, Boldyryeva H, Pihosh Y, Slavinska D, Noskova L, Skuciova M, Lisa V, Biederman H 2009, "Nanocomposite Ti/hydrocarbon plasma polymer films from reactive magnetron sputtering as growth support for osteoblast-like and endothelial cells", *Journal of Biomedical Materials Research Part A*, vol. 88, no. 4, pp. 952-66. doi: 10.1002/jbm.a.31918.
25. Lopez-Santos C, Colaux JL, Laloy J, Fransolet M, Mullier F, Michiels C, Dogné JM, Lucas S 2013, "Bioactivity and hemocompatibility study of amorphous hydrogenated carbon coatings produced by pulsed magnetron discharge", *Journal of Biomedical Materials Research Part A*, vol. 101, no. 6, pp. 1800-1812. doi: 10.1002/jbm.a.34489.
26. Seidenstuecker M, Weber J, Latorre SH, Straub B, Matthes U, Friedrich C, Mayr HO, Bernstein A 2019, "Alendronate release from UHMWPE-based biomaterials in relation to particle size of the GUR powder for manufacturing", *Materials (Basel)*, vol. 12, no. 11, article no. 1832. doi: 10.3390/ma12111832.

27. Fowkes FM 1964. Attractive Forces at Interfaces. *Industrial & Engineering Chemistry Research*. vol. 56, no. 12, pp. 40–52, doi: 10.1021/ie50660a008

28. Lowry OH, Rosebrough NJ, Farr AL, Randall RJ 1951, "Protein measurement with the Folin phenol reagent", *Journal of Biological Chemistry*, vol. 193, pp. 265–275. doi: 10.1016/S0021-9258(19)52451-6

29. Schroeder A, Francz G, Bruinink A, Hauert R, Mayer J, Wintermantel E 2000, "Titanium containing amorphous hydrogenated carbon films (a-C: H/Ti): surface analysis and evaluation of cellular reactions using bone marrow cell cultures *in vitro*", *Biomaterials*, vol. 21, no. 5, pp. 449-56. doi: 10.1016/s0142-9612(99)00135-0.

30. Rothammer B, Neusser K, Marian M, Bartz M, Krauß S, Böhm T, Thiele S, Merle B, Detsch R, Wartzack S 2021, "Amorphous carbon coatings for total knee replacements-Part I: Deposition, cytocompatibility, chemical and mechanical properties", *Polymers (Basel)*, vol. 13, no. 12, article no. 1952. doi: 10.3390/polym13121952.

31. Rothammer B, Marian M, Neusser K, Bartz M, Böhm T, Krauß S, Schroeder S, Uhler M, Thiele S, Merle B, Kretzer JP, Wartzack S 2021, "Amorphous carbon coatings for total knee replacements-Part II: Tribological behavior", *Polymers (Basel)*, vol. 13, no. 11, article no. 1880. doi: 10.3390/polym13111880.

32. Major R, Gawlikowski M, Plutecka H, Surmiak M, Kot M, Dyner M, Lackner JM, Major B 2021, "Biocompatibility testing of composite biomaterial designed for a new petal valve construction for pulsatile ventricular assist device", *Journal of Materials Science: Materials in Medicine*, vol. 32, no. 9, article no. 118. doi: 10.1007/s10856-021-06576-w.

33. Thukkaram M, Vaidulych M, Kylián O, Hanuš J, Rigole P, Aliakbarshirazi S, Asadian M, Nikiforov A, Van Tongel A, Biederman H, Coenye T, Du Laing G, Morent R, De Wilde L, Verbeken K, De Geyter N 2020, "Investigation of Ag/a-C:H nanocomposite coatings on titanium for orthopedic applications", *ACS Applied Materials & Interfaces*, vol. 12, no. 21, article no. 23655-23666. doi: 10.1021/acsami.9b23237.

34. Milan PB, Khamseh S, Zarrintaj P, Ramezanzadeh B, Badawi M, Morisset S, Vahabi H, Saeb MR, Mozafari M 2020, "Copper-enriched diamond-like carbon coatings promote regeneration at the bone-implant interface", *Heliyon*, vol. 6, no. 4, article no. e03798. doi: 10.1016/j.heliyon.2020.e03798.

35. Secker TJ, Hervé R, Zhao Q, Borisenko KB, Abel EW, Keevil CW 2012, "Doped diamond-like carbon coatings for surgical instruments reduce protein and prion-amyloid biofouling and improve subsequent cleaning", *Biofouling*, vol. 28, no. 6, pp. 563-569. doi: 10.1080/08927014.2012.698387.

36. Chai F, Mathis N, Blanchemain N, Meunier C, Hildebrand HF 2008, "Osteoblast interaction with DLC-coated Si substrates", *Acta Biomaterialia*, vol. 4, no. 5, article no. 1369-81. doi: 10.1016/j.actbio.2008.04.011.

37. Poulsson AH, Mitchell SA, Davidson MR, Johnstone AJ, Emmison N, Bradley RH 2009, "Attachment of human primary osteoblast cells to modified polyethylene surfaces", *Langmuir*, vol. 25, no. 6, pp. 3718-3727. doi: 10.1021/la801820s.

38. Posa F, Di Benedetto A, Cavalcanti-Adam EA, Colaianni G, Porro C, Trotta T, Brunetti G, Lo Muzio L, Grano M, Mori G 2018, "Vitamin D promotes MSC osteogenic differentiation stimulating cell adhesion and αVβ3 expression", *Stem Cells International*, vol. 2018, article no. 6958713. doi: 10.1155/2018/6958713.

39. Peng Y, Qu R, Yang Y, Fan T, Sun B, Khan AU, Wu S, Liu W, Zhu J, Chen J, Li X, Dai J, Ouyang J 2023, "Regulation of the integrin αVβ3- actin filaments axis in early osteogenic differentiation of human mesenchymal stem cells under cyclic tensile stress", *Cell Communication and Signaling*, vol. 21, no. 1, article no. 308. doi: 10.1186/s12964-022-01027-7.

40. Sagomonyants KB, Jarman-Smith ML, Devine JN, Aronow MS, Gronowicz GA 2008, "The *in vitro* response of human osteoblasts to polyetheretherketone (PEEK) substrates compared to commercially pure titanium", *Biomaterials*, vol. 29, no. 11, pp. 1563-1572. doi: 10.1016/j.biomaterials.2007.12.001.
41. Zhang Y, Liu L, Li M, Wang S, Fu J, Yang M, Yan C, Liu Y, Zheng Y 2025, "Dose-dependent enhancement of in vitro osteogenic activity on strontium-decorated polyetheretherketone", *Scientific Reports*, vol. 15, no. 1, article no. 3063. doi: 10.1038/s41598-025-86561-3.
42. Cvrček L, Krčil J, Musílková J, Musílková V, Bačáková L, Nehasil V, Denk F, Čejka Z 2022, "Nanostructured TiNb coating improves the bioactivity of 3D printed PEEK", *Materials and Design*, vol. 224, article no. 111312. doi: 10.1016/j.matdes.2022.111312.
43. Tanaka Y, Maruo A, Fujii K, Nomi M, Nakamura T, Eto S, Minami Y 2000, "Intercellular adhesion molecule 1 discriminates functionally different populations of human osteoblasts: characteristic involvement of cell cycle regulators", *Journal of Bone and Mineral Research*, vol. 15, no. 10, art. no. 1912-1923. doi: 10.1359/jbmr.2000.15.10.1912.
44. Lavigne P, Benderdour M, Shi Q, Lajeunesse D, Fernandes JC 2005, "Involvement of ICAM-1 in bone metabolism: a potential target in the treatment of bone diseases?", *Expert Opinion on Biological Therapy*, vol. 5, no. 3, pp. 313-320. doi: 10.1517/14712598.5.3.313.
45. Kong L, Yang X 2020, "Study of intercellular adhesion molecule-1 (ICAM-1) in bone homeostasis", *Current Drug Targets*, vol. 21, no. 4, pp. 328-337. doi: 10.2174/1389450120666190927122553.
46. Lisignoli G, Toneguzzi S, Piacentini A, Cristino S, Cattini L, Grassi F, Facchini A 2004, "Recruitment and proliferation of T lymphocytes is supported by IFNgamma- and TNFalpha-activated human osteoblasts: Involvement of CD54 (ICAM-1) and CD106 (VCAM-1) adhesion molecules and CXCR3 chemokine receptor", *Journal of Cellular Physiology*, vol. 198, no. 3, article no. 388-98. doi: 10.1002/jcp.10427.
47. Štefančík M, Válková L, Veverková J, Balvan J, Vičar T, Babula P, Mašek J, Kulich P, Pávková Goldbergová M 2021, "Ni and TiO(2) nanoparticles cause adhesion and cytoskeletal changes in human osteoblasts", *Environmental Science and Pollution Research International*, vol. 28, no. 5, pp. 6018-6029. doi: 10.1007/s11356-020-10908-8.
48. Chico B, Pérez-Maceda BT, San-José S, Escudero ML, García-Alonso MC, Lozano RM 2022, "Wettability, corrosion resistance, and osteoblast response to reduced graphene oxide on CoCr functionalized with hyaluronic acid", *Materials (Basel)*, vol. 15, no. 7, article no. 2693. doi: 10.3390/ma15072693.
49. Kosmidis K, Ehsan K, Pitzurra L, Loos B, Jansen I 2023, "An *in vitro* study into three different PRF preparations for osteogenesis potential", *Journal of Periodontal Research*, vol. 58, no. 3, pp. 483-492. doi: 10.1111/jre.13116.
50. Liu JF, Tsao YT, Hou CH 2016, "Fractalkine/CX3CL1 induced intercellular adhesion molecule-1-dependent tumor metastasis through the CX3CR1/PI3K/Akt/NF-κB pathway in human osteosarcoma", *Oncotarget*, vol. 8, no. 33: pp. 54136-54148. doi: 10.18632/oncotarget.11250.